Modelling the behaviour of composite sandwich structures when subject to air-blast loading

H. Arora, P.A. Hooper, P. Del Linz, H. Yang, S. Chen and J.P. Dear*
Department of Mechanical Engineering, Imperial College London, SW7 2AZ

ABSTRACT

Large-scale glass fibre reinforced polymer (GFRP) and carbon fibre reinforced polymer (CFRP) sandwich structures (1.6 m × 1.3 m) were subject to explosive air blast (100 kg TNT equivalent) at stand-off distances of 14 m. Digital image correlation (DIC) was used to obtain full-field data for the rear-face of each deforming target. A steel plate of comparable mass per unit area was also subjected to the same blast conditions for comparison. The experimental data was then verified with finite element models generated in Abaqus/Explicit. Close agreement was obtained between the numerical and experimental results, confirming that the CFRP panels had a superior blast performance to the GFRP panels. Moreover all composite targets sustained localised failures (that were more severe in the GFRP targets) but retained their original shape post blast. The rear-skins remained intact for each composite target with core shear failure present.

Keywords: Air blast, Shock, Sandwich Structures, Composites.

1. INTRODUCTION

The recent advancements in composite manufacturing have occurred predominantly in the aerospace, marine, automotive and related industries. Whereas, formerly, naval vessels were constructed from steel, composites provide a significant weight reduction and increase in stealth properties whilst maintaining high strength properties. Composites behave in different ways to steels, which have predominantly isotropic properties. This leads to a need for new design protocols to be developed for the safety of naval craft. Glass fibre reinforced polymer (GFRP) and carbon fibre reinforced polymer (CFRP) composites are quickly finding application in the construction of naval structures as well as new polymer fibre hybrids. These materials can be subject to increasingly demanding and varied conditions during service. In a military context, blast loads represent the an threat to a structure. The research presented in this paper focuses on air-blast loading of sandwich composite panels and finite element (FE) modelling of these air-blast conditions.

There have been numerous investigations into blast loading of structures using open air charges and underwater charges. Several studies have investigated dynamic deformations due to explosive blast loading on plates. Neuberger [1, 2] highlighted several early studies, which classified failure modes of structures under impulse loading, from large inelastic

*Corresponding author: Prof. John P. Dear Email: j.dear@imperial.ac.uk
Tel:+44 207 594 7086

deformation to tearing and shear failure at the supports. Neuberger also highlighted various studies investigating the scaling effects for comparison of similar blast events using different explosive mass or specimen distance to quantify material response. These studies observed the effect of air-blast [1] and underwater charges [2] on clamped circular plates and the validity of scaled testing. Several earlier studies have also investigated the dynamic deformations due to explosive blast loading on plates. Menkes and Opat [3] classified failure modes of structures under impulse loading, from large inelastic deformation to tearing and shear failure at the supports. Nurick, amongst others has conducted extensive studies over the years investigating plate response to blast loading (summarised in reference [4]). For instance the types of failures described by Menkes and Opat have been investigated further by Nurick, Olsson et al. [5], in particular the significant effects of the boundary conditions for the purpose of predicting tearing in steel plates have been highlighted in reference [6]. Cantwell, Nurick and Langdon et al. have continued similar experimental investigations and analysis into composite behaviour under blast conditions [7–9]. Rather than using explosives to generate shocks, shock tubes have been shown to be a favourable alternative used extensively in shock/blast simulation studies. Tekalur et al. [10–12] have experimentally studied the effect of blast loading using shock tubes and controlled explosion tubes loading on E-glass fibre based composites and other materials.

Research has been conducted in the past on the blast resistance of GFRP sandwich panels of varying core thicknesses [13]. The results showed the strong influence of this parameter on the behaviour of the panels, as their stiffness was significantly higher for thicker cores. The research presented in this paper adds to previous research, focussing on full-scale air-blast experimentation conducted on GFRP and CFRP sandwich composite panels. These panels were of similar mass per unit area and overall thickness. This provided for a direct comparison between these two forms of construction. An additional experiment was also performed comparing these composite materials to traditional shipbuilding steel plate of similar mass per unit area. The blast experiments were also simulated using FE analysis. The aim was to evaluate these materials experimentally in terms of blast response; damage sustained; and to assess the behaviour further using FE models to represent the blast loading on the targets.

2. BLAST EXPERIMENTS

2.1. MATERIALS

In this set of experiments, GFRP and CFRP sandwich panels were subject to full-scale air-blast loading from 100 kg Nitro-methane explosive charges (100 kg TNT equivalent) to observe the deformation and damage development during the event. The composite materials (1.6 m × 1.3 m) were sourced from S.P. Gurit, manufactured by P.E. Composites. Whilst different GFRP and CFRP skins were employed, all composite panels used the same 25 mm thick closed-cell M130 Corecell^{TM} styrene acronitrile (SAN) foam core. In total, five targets were evaluated. There were four composite sandwich panels: two with GRRP skins, denoted G25a and G25b; and two with CFRP skins, denoted C25a and C25b. In addition to the four sandwich composite targets, one steel sheet, 3 mm mild steel composition EN-10025-2-05-S275JR-AR was also evaluated, denoted S3a. The GFRP and CFRP-skinned panels had equivalent mass per unit area, ~ 17 kg/m^2 (all samples weighed in the region of 35 kg). The steel plate also had a near equivalent mass per unit area as the composite sandwich panels, albeit slightly heavier at ~ 23 kg/m^2.

The GFRP panels were constructed using two plies of 0°/90°/ ± 45° E-glass quadriaxial skins (material code: QE1200) on a 25 mm SAN foam core (material code: M130). The

Table 1 Material properties of the sandwich panel constituent elements.

Material property	**QE1200**	**RC245T**	**RC380T**	**M130**
Density (kg/m^3)	1750	1393	1393	140
Tensile modulus (GPa)	17	50	11	0.18
Compressive modulus (GPa)	—	—	—	0.17
Tensile strength (MPa)	260	471	—	2.85
Compressive strength (MPa)	200	316	—	2.31
Shear modulus (MPa)	6500	3150	23600	59
Tensile failure strain (%)	1.5	0.9	—	1.6

CFRP equivalent panels consisted of skins with two repeat layers of two plies 0°/90° carbon (material code: RC245T) and two of plies ± 45° carbon (material code: RC380T) on a 25 mm SAN foam core (material code: M130). The steel panel was fabricated from 3 mm thick mild steel plate. All sandwich constructions were infused with Ampreg 22, an epoxy resin. Material properties are summarised in Table 1.

2.2. BLAST EXPERIMENTAL DESIGN AND INSTRUMENTATION

Explosive charges were used to simulate moderate to large blast loads in close proximity to naval vessels above the waterline. The charge weight and stand-off were determined with a finite element simulation of the GFRP panel setting an observed strain threshold to a given blast impulse of 1.5% strain, where damage is expected to initiate. This process was outlined previously in more detail in reference [14]. This equated to a 100 kg of TNT equivalent charge set at a 14 m stand-off distance from the panels. Three explosive charges were employed in total. The panels were located in a concrete cubicle with a steel front. Figure 1 shows the geometry of the structure. Care was taken to ensure symmetric loading conditions on the panels, ensuring that the charge was located at mid-height and at 90° from the centre of the cubicle (see Figure 2 for details). Two targets were evaluated during each blast, tested side-by-side in this purpose built concrete/steel test fixture.

Digital image correlation (DIC) was employed to record full-field displacement and in-plane strain data for the rear-face of each of the panels evaluated. Here two high-speed video cameras (Photron SA3s) were positioned behind each of the two 1.6 m × 1.3 m speckled targets

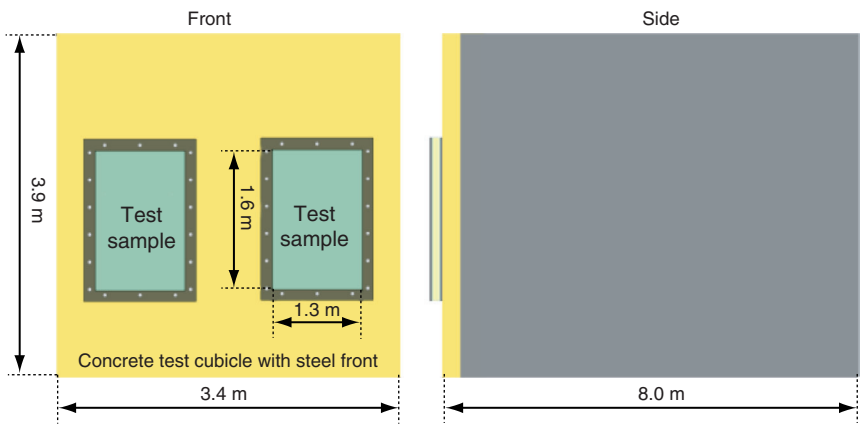

Figure 1 Concrete test cubicle used for testing up to two samples at a time.

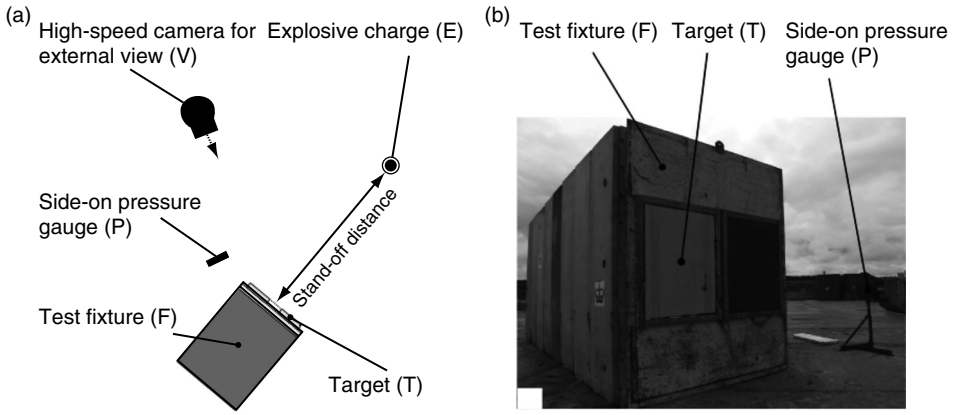

Figure 2 Blast configuration for tests: (a) schematic diagram and (b) image of the test set-up. Featured in each diagram are: target to be tested (T), test cubicle (F), high-speed camera and its relative location on the test pad (V), pressure sensor arrangements (P) and Nitro-methane explosive charge (E).

(black speckles on a matte white background applied to the rear face), sampling at 2000 fps at full resolution (1024 × 1024 pixels), similar to the set up described in references [13, 14, 15]. The four high-speed cameras were positioned behind the targets in vertical pairs. The sampling frequency was determined using a single degree of freedom method outlined in reference [16] to estimate the time taken for the panel to reach the point of maximum deflection. The system was calibrated before testing to allow the recorded images to be processed in ARAMIS (produced by GOM mbH), the DIC software used to perform the image correlation calculations. This camera arrangement was housed in the test cubicle described previously.

An additional high speed camera was located outside the test cubicle to observe the pressure wave effects on the front-face of the targets and test fixture. A pressure gauge was positioned next to the test cubicle at the same stand-off distance from the charge to record the overpressure, P, generated by each blast. Figure 2 shows the layout of the test pad and an image of the test cubicle.

2.3. RESULTS

The first two 100 kg TNT equivalent blasts were used to compare CFRP-skinned composite sandwich panel (C25a and C25b) with the GFRP-skinned composite sandwich panels (G25a and G25b). Both experiments showed similar response, forming the same visible damage post-test. The second test is presented (for G25b and C25b). Figure 3 shows the front-face deformation at regular intervals for this experiment. This shows the progressive deformation and eventual skin damage inflicted on the panel by the blast, where the peak overpressure, P_{max}, was equal to 250 kPa and positive wave duration of the blast, τ_d, was equal to 12.0 ms. A front skin crack is seen to originate from the top right-hand edge of the GFRP panel at approximately 19 ms into the blast event and propagate down the left-hand side of the target. Figure 4 and Figure 5 shows a summary of the data recorded for this blast (100 kg Nitro-methane at 14 m stand-off) for the G25b and C25b respectively. Figure 4(b) and Figure 5(b) show central out-of-plane displacement (using DIC data) of the target sandwich panel with the pressure-time trace overlaid. This helps to characterise the blast in terms of the target response relative to its loading. The regime of this test can be referred to

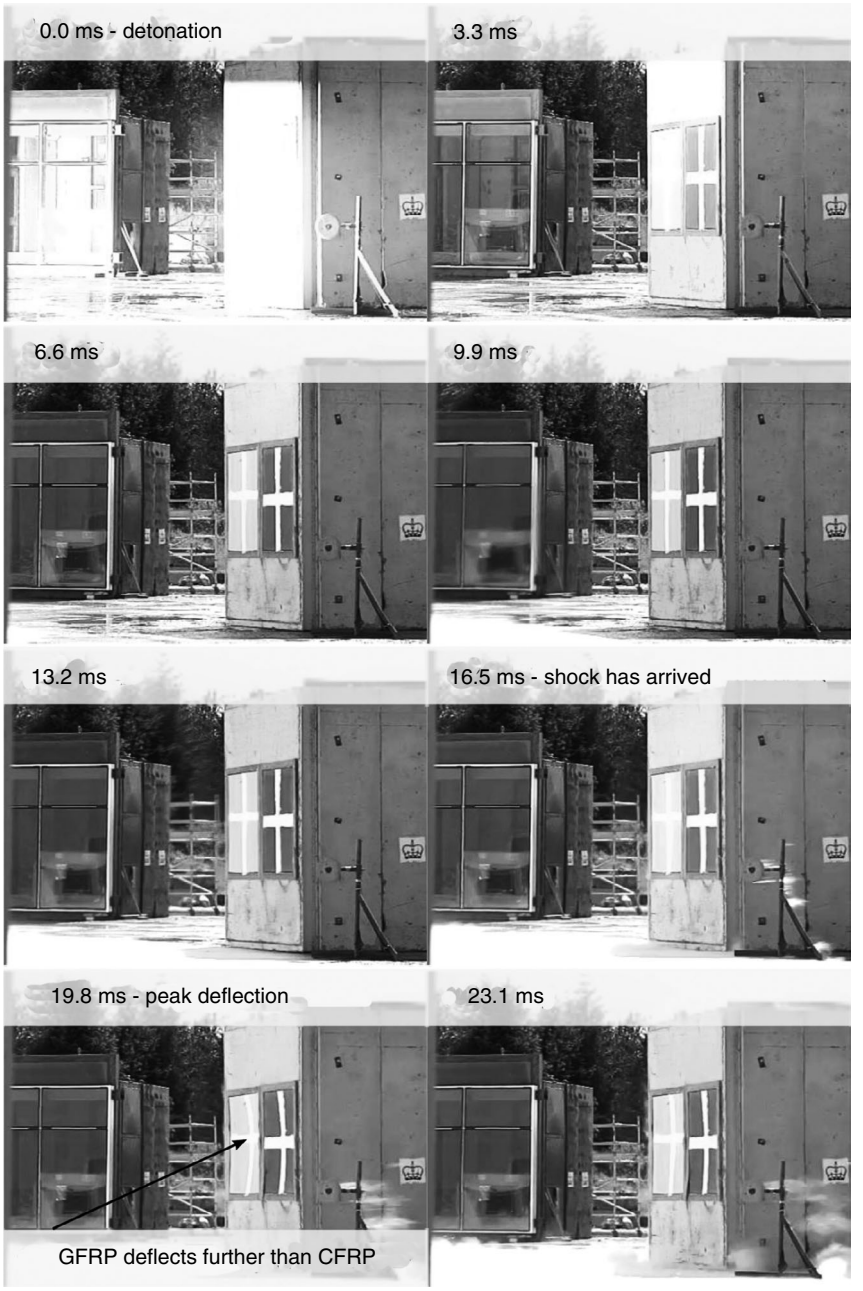

Figure 3 Images of shock wave progression and front-face deformation of G25b and C25b. Images are shown from the detonation (0 ms) through the air shock wave arrival at target (15 ms) until targets begin their first rebound.

as dynamic, based on reference [17]. The contour plots shown in Figure 4(a) and Figure 5(a) show the transient response of the target with respect to out-of-plane displacement (U_z) of the rear face, in-plane maximum principal strain ($\varepsilon_{\max}$) and shear strain (ε_{xy}).

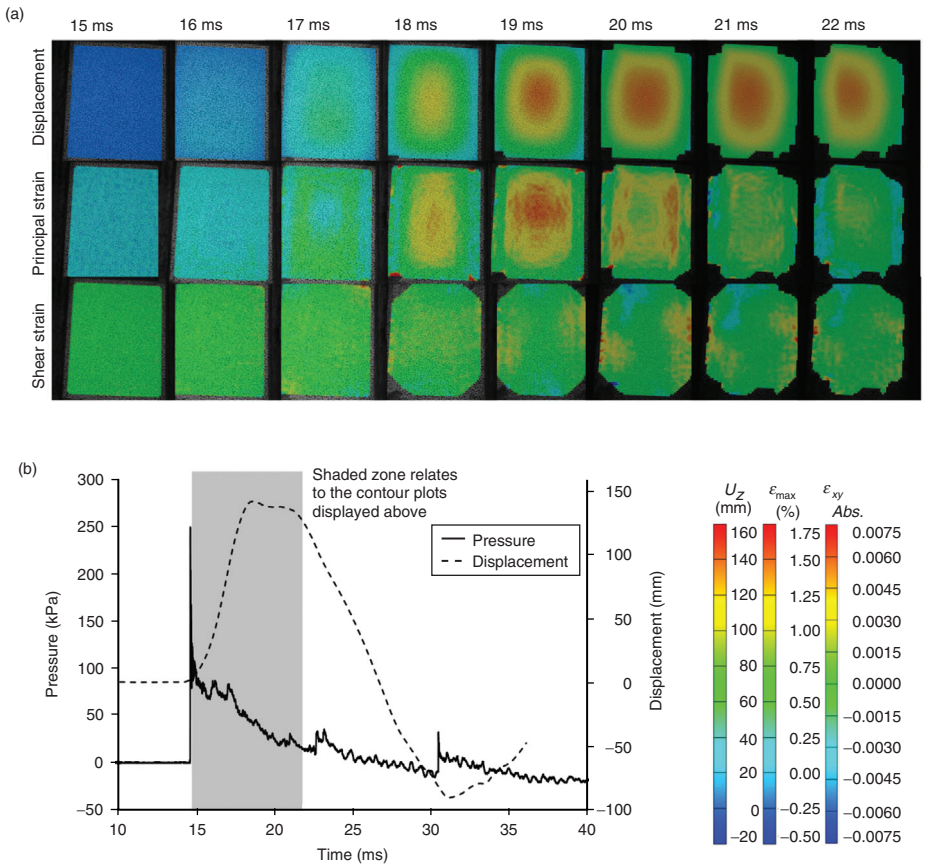

Figure 4 Blast summary for 100 kg TNT equivalent at 14 m stand-off from G25b including: (a) DIC analysis and (b) a plot of pressure-time and displacement-time using DIC centre point measurements. The DIC analyses features contour plots of out-of-plane displacement, maximum principal strain and shear strain, corresponding to different stages in the graphical plot.

The GFRP (Figure 4(a)) contour plots all indicate a uniform and symmetrical response across the panel up until maximum out-of-plane displacement, $U_{z,\max}$, at 19 ms is reached. After this point front-face and core damage has been sustained, causing the distorted nature of the displacement plot around $U_{z,\max}$. This coincides with the time period over which the crack was observed to initiate and propagate in Figure 3. $U_{z,\max}$ was found to be 140 mm and $\varepsilon_{\max}$ peaked in the region of ~ 1.6% prior to the crack developing.

By comparison, C25b, in Figure 5, is observed to deflect noticeably less than G25b. As discussed previously, a considerable front skin crack was seen to form in G25b, however C25b showed no major observable skin failure. A fine crack was observed to form towards one of the panel edges and core shear failure was still observed to a similar severity as for G25b. Figure 5 shows that the stiffer carbon skins minimise $U_{z,\max}$ to 107 mm (compared to 135 mm for G25b). The contour plots in Figure 5(a) show a larger central flat region than G25b. This is because more of the blast energy was distributed throughout the structure in C25b, causing less severe but more widespread core cracking. Conversely G25b did not

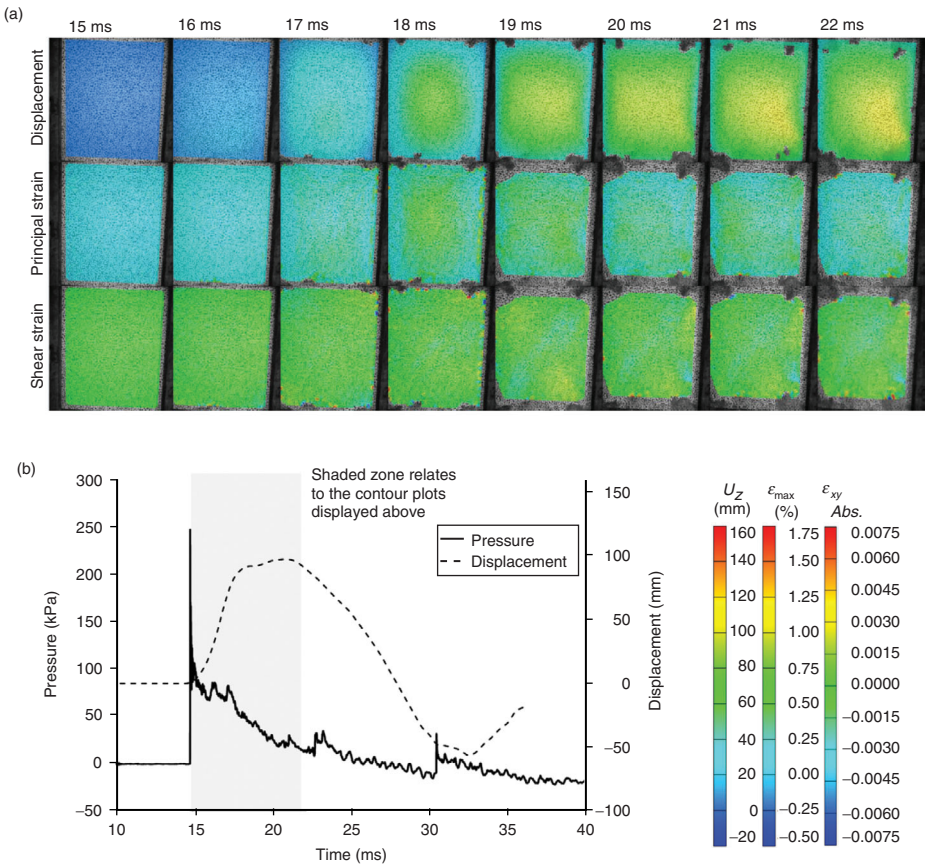

Figure 5 Blast summary for 100 kg TNT equivalent at 14 m stand-off from C25b including: (a) DIC analysis and (b) a plot of pressure-time and displacement-time using DIC centre point measurements. The DIC analyses features contour plots of out-of-plane displacement, maximum principal strain and shear strain, corresponding to different stages in the graphical plot.

distribute the blast energy quick enough throughout the entire structure leading to a major localised failure of the front skin and core. This type of damage mechanism (core cracking) accounts for the elongated return of C25b since if the integrity of the core structure is compromised by multiple core cracks, the flexural rigidity would reduce. Therefore the frequency of response would decrease (causing the period of response to increase). This was observed with the time taken for the panel to return to its original position, which took an extra millisecond in the carbon-skinned panel compared to the glass-skinned panel. This extended response time absorbed the blast energy over a longer time period, resulting in a lower observed deflection $U_{z,\max}$ (107 mm) and principal strain $\varepsilon_{\max}$ (~ 0.8%).

Upon post inspection, the inter-laminar skin failure and severe front-ply fibre breakage of G25b was confirmed. For both panels the core suffered cracking from front skin to rear skin but the rear skin remained intact. Figure 6 shows an overview of the damage observed by the two panels. The core damage initiated for G25b in transition regions from constraint to regions of deflecting panel. This is where the stress state caused by the restraint and the

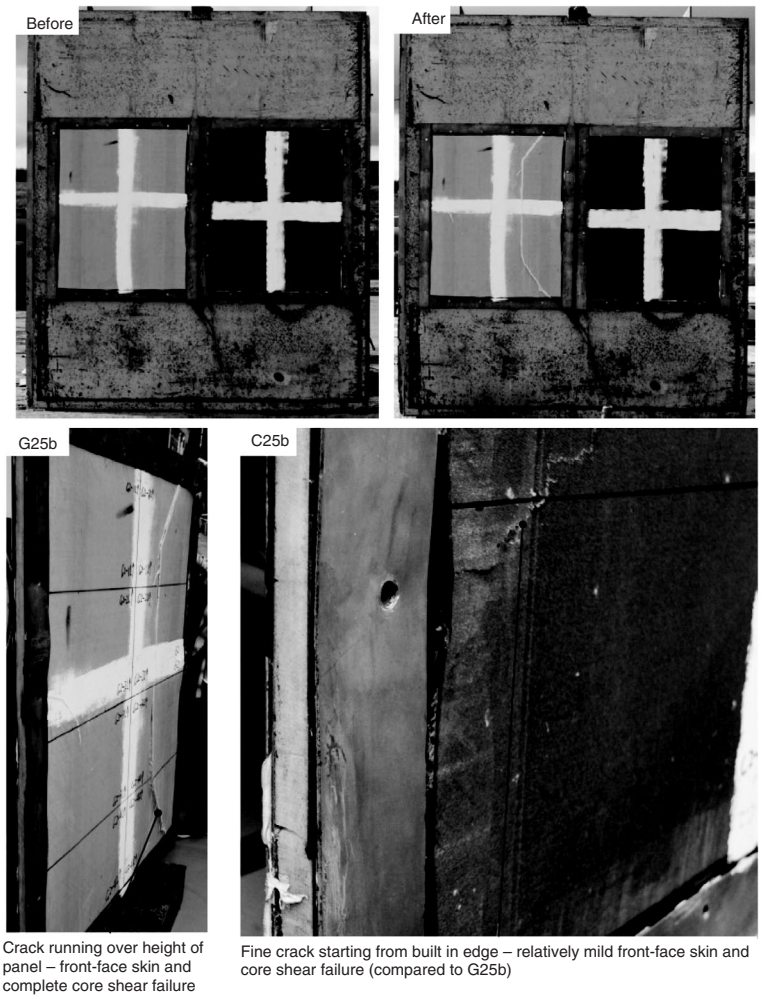

Figure 6 Comparison of damage showing more skin/core damage in G2 compared to C2.

impulsive loading promotes failure initiation. The lack of sufficient distribution of energy lead to global propagation of the crack in the GFRP panels compared to the CFRP panels, which have small areas of skin cracking (which was seen to initiate from the stress concentration at the bolt hole - see Figure 6).

The third blast conducted during this set of experiments involved a mild steel plate (S3a). Figure 7 shows the external view captured of the deformation process. Figure 8 gives a summary in the same fashion as for G25b and C25b. From the plot in Figure 8(b) there is close to linear initial portion of response, however at around 20 ms, S3a pulls out from six bolt holes. This dissipated a lot of energy and relieved the intensity of the oncoming pressure wave providing clearing for the blast wave, hence the sharp decrease in gradient of the displacement-time plot.

The displacement-time curve for the steel plate is seen to decrease in gradient steadily until it plate. The contour plots in Figure 8 only show the deformation within the time period shown for that of G25b and C25b and so do not show the full response of the target. Figure 9 shows

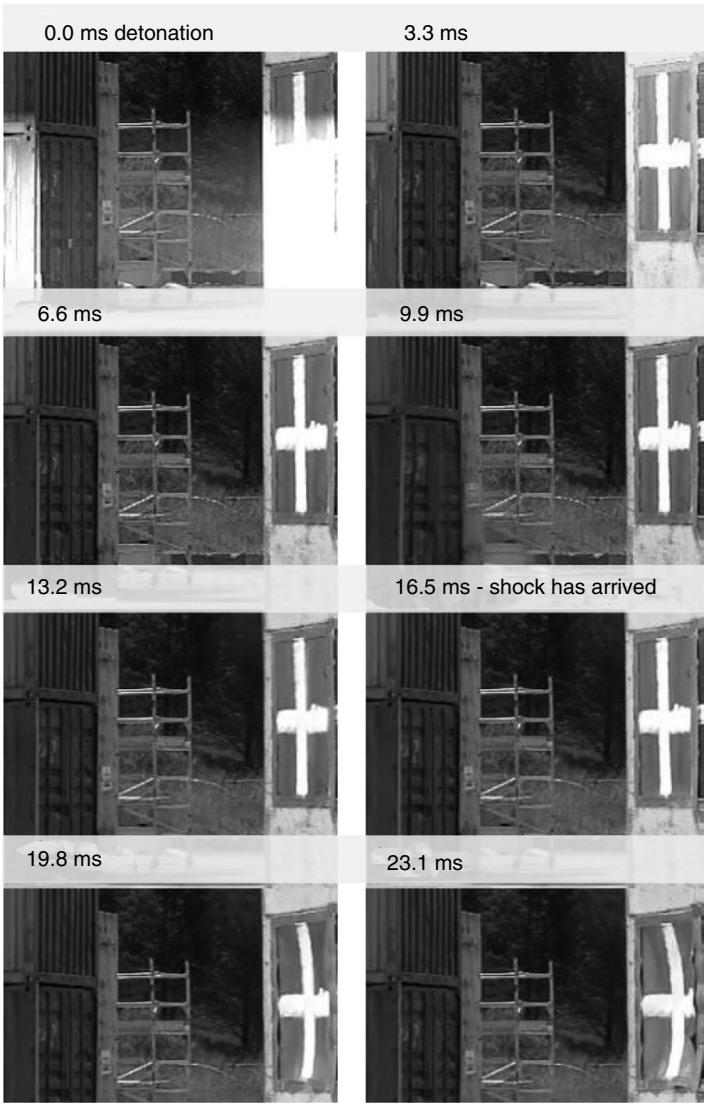

Figure 7 Images of shock wave progression and front-face deformation of S3a. Images are shown from the detonation (0 ms) through the air shock wave arrival at target (15 ms) until the target begins its first rebound.

a stage later in the deformation process at 24.5 ms after detonation. This shows that the panel continued to deform significantly further than the sandwich structures. Moreover S3a folded and crumpled in the regions between the bolt holes where high shear stresses occur. S3a had a peak deflection which was 270 mm, which is considerable more than GFRP and CFRP skinned sandwich panels. A deflection of approximately 120 mm was attained prior to bolt shear, which dissipated some energy and also relieved some of the blast pressure.

The major principal strain peaks at approximately 1.1% at 24.5 ms for the steel plate. The damage sustained by S3a is featured in Figure 10, showing the final deformed profile relative to its original at profile.

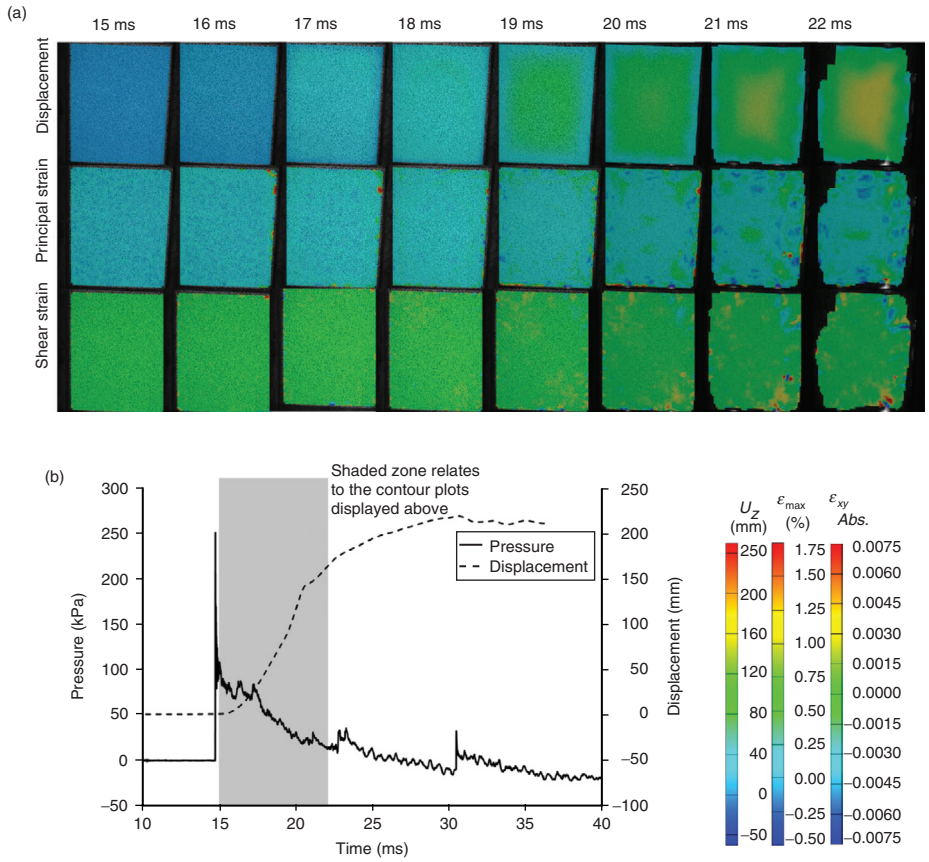

Figure 8 Blast summary for 100 kg TNT equivalent at 14 m stand-off from S3a including: (a) DIC analysis and (b) a plot of pressure-time and displacement-time using DIC centre point measurements. The DIC analyses features contour plots of out-of-plane displacement, maximum principal strain and shear strain, corresponding to different stages in the graphical plot.

2.4. ANALYSIS

The DIC data was used to plot the deflected profile of a central section of the panels and to calculate average deflection velocities. Figure 11 shows the cross-sectional deformation of G25b during the blast. There was a uniform forward (positive) stroke, however, due to the compromised integrity of the skin and core, there was an augmented return stroke. The core crack seemed to initiate in the early stages again at ~1.5 ms after impact of the air shock which was 16.5 ms after detonation.

The deformation profile of C25b is given in Figure 12. It is interesting to compare these two graphs bearing in mind the nature of visible damage observed in Figure 6. As stated previously, the higher bending stresses cause shear cracks to initiate in the early stages of the two target's deformation cycles. However since the GFRP structure provides less resistance to the impact of the air shock, the severity of damage increases faster than in the CFRP structure. Furthermore the average velocity of the target deflection was 40 m/s in G25b compared to 25 m/s in C25b. This extra kinetic energy in the GFRP target

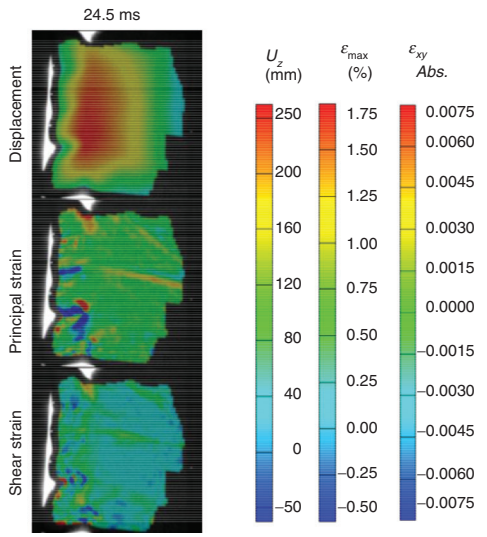

Figure 9 A frame taken from the latter stages of the panel deformation, showing the permanently deformed contours of S3a. The DIC analysis gives a contour plot of out-of-plane displacement, maximum principal strain and shear strain, corresponding to 24.5 ms after detonation.

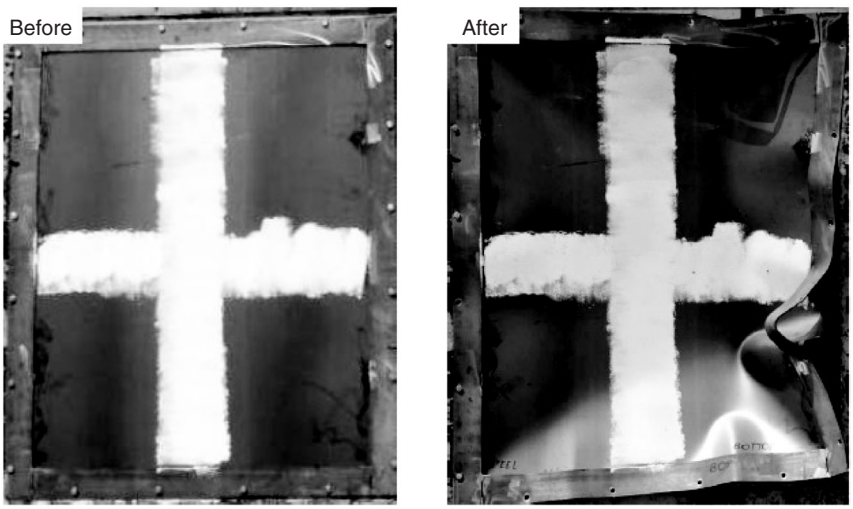

Figure 10 Before and after images taken of the front-face view of S3a which was subject to a charge of 100 kg TNT equivalent at stand-off of 14 m.

(momentum) leads to greater stresses induced in the skins and across the core upon recovery (rebound), causing the core crack to propagate to complete failure (front skin-to-rear skin core shear failure). In the case of G25b this lead to fibre breakage all along this crack at the point of peak deflection. The CFRP target, C25b, distributed the blast energy more effectively through the panel and responded with a greater resistance to the impact.

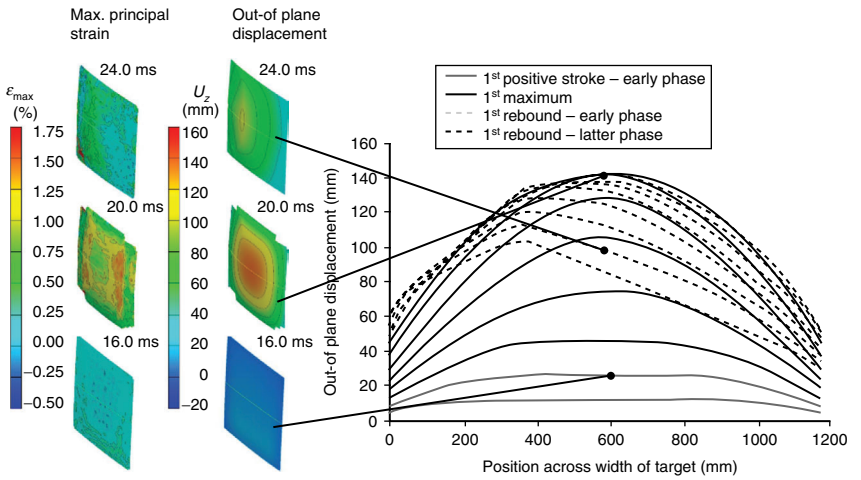

Figure 11 Displacement data taken across a horizontal section running through the point of maximum deflection for the panel G25b during blast loading (100 kg TNT equivalent at 14 m stand-off). Data displayed for regular intervals of 0.5 ms from 15 ms after detonation. Solid lines show displacement profile up to maximum deflection and dotted lines show subsequent return.

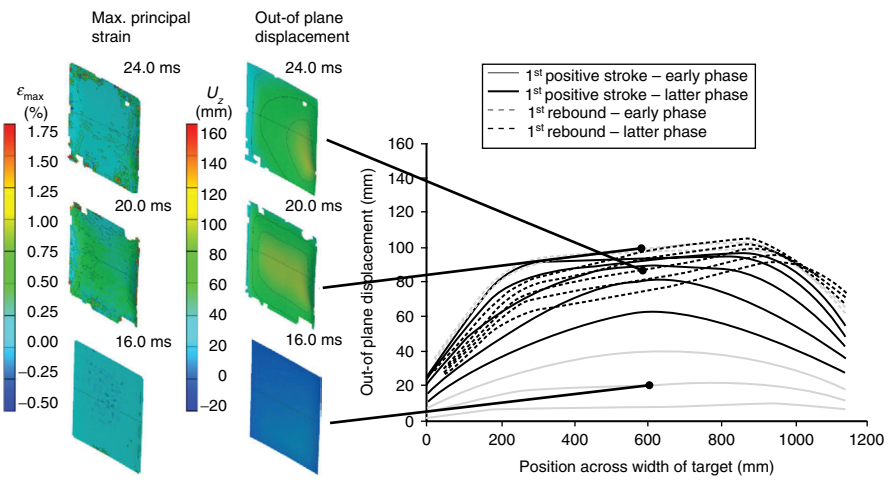

Figure 12 Displacement data taken across a horizontal section running through the point of maximum deflection for the panel C25b during blast loading (100 kg TNT equivalent at 14 m stand-off). Data displayed for regular intervals of 0.5 ms from 15 ms after detonation. Solid lines show displacement profile up to maximum deflection and dotted lines show subsequent return.

It gained less kinetic energy, which was dissipated on the rebound strike without any global skin failures. The core cracks are clearly noticeable from Figure 12. Once the centre of the target reached $U_{z,\max}$, the remaining momentum carried the edges of the panel forward, unrestrained due to the loss in integrity of the core, leading to this flattening out observed of the deformed profile.

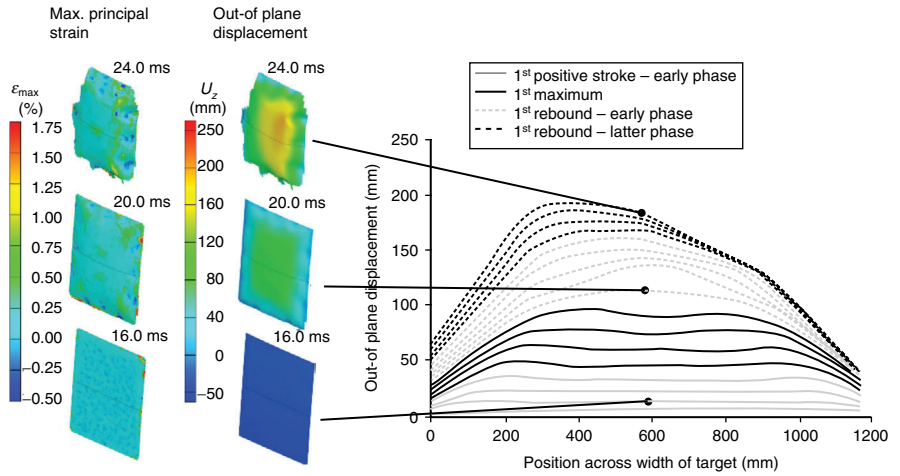

Figure 13 Displacement data taken across a horizontal section running through the point of maximum deflection for the steel plate S3a during blast loading (100 kg TNT equivalent at 14 m stand-off). Data displayed for regular intervals of 0.5 ms from 15 ms after detonation. Solid lines show displacement profile up to bolt shear and dotted lines show subsequent deformation.

Finally, for the steel plate (S3a) data is analysed to give a direct comparison to the GFRP and CFRP sandwich panels. The steel plate exhibits the classic impulsive behaviour, with the central flattened region. Extensive work on steel plates and their failure modes has been conducted by Nurick et al., particularly reference [5] discusses the three main failure modes expected to occur under blast conditions. These modes are large inelastic ductile deformation (mode I), tensile tearing at the supports (mode II) and transverse shear failure at the supports (mode III). Referring to Figure 13, the extended duration of the deformation cycle with the flattened region implies the plate did not have sufficient time to reach the mode I failure mechanism and so the deformations concentrate around the edges of the central region (similar observations were made on 240 mm × 240 mm size samples in [5]). This blast caused bolt shear to occur on one side and this is clear from Figure 13 causing the bias on the deformed profile. The plate was moving at an average velocity of 25 m/s at the point of bolt shear, causing a jump in the central point velocity (up to 31 m/s). Then the remaining tail of the pressure pulse and momentum of the plate causes the plate to continue with large plastic deformations. The steel plate is heavier than the composite sandwich panels, therefore these velocities of deformation and amplitudes of deflection are considerable from a blast mitigation point of view. These observations indicate, based on these design criteria, that the fibre reinforced polymer composite (FRPC) sandwich materials are more blast tolerant than shipbuilding steel plate.

3. NUMERICAL MODELLING OF PANEL RESPONSE

Finite element models have been produced and used during the course of these blast studies employing Abaqus/Explicit 6.10 as either a predictive or evaluative tool. They have been used during the design process, when planning the sample construction to test against which blast scenario (charge size, stand-off and support conditions). Post-test, these models have been evaluated against experimental data and in some cases extended to explain any subtle

or significant differences between the real (experimental) and the ideal (numerical simulation) blast cases.

3.1. METHOD

Initially a 3D solid continuum element model was generated with the plate geometry sectioned into its composite constituent layers. The target was loaded with a uniformly distributed pressure load with amplitude-time characteristic to a given blast. Mesh refinement was such that the core had five elements through thickness and the skins were kept as one element thick as their through thickness contributions to the panel deformation could be neglected (bending taken into account not transfer of shear or compressive stresses). Mesh refinement studies were conducted to ensure high spatial resolution of the result is maintained throughout the analysis. Areal mesh refinement was such that coverage was approximately one element per 10 mm × 10 mm area. This resulted in approximately 125000 element model being generated of C3D8R elements. This model was then simplified to a 2D shell element model for computational efficiency and geometric simplicity. The number of elements reduced from 125000 elements to 2600 S4R elements for the plate area, 1.6 m × 1.3 m. This simplification was done since the correlation of in-plane surface strains and peak deflection between the 3D solid continuum element model and 2D shell element model was strong. Given these are the measured quantities from the experiments and were captured sufficiently well subsequent work proceeded with the 2D shell model for this investigation. It should be noted that the move to a 2D shell model precludes the observation of significant through-thickness stresses. However, as no core crushing was observed during air-blast experiments, this was considered acceptable for this application.

There are other effects which should be recognised and can be included in the models to improve the details of the analysis such as, the non-uniformity of the pressure distribution arising from target geometry and ground reflections. The pressure distribution was studied using Air3D, a computational fluid dynamics software package for predicting blast loads. To summarise the basics of the blast wave interaction with the target structure, there are two main factors to be considered: the duration and magnitude of the pressure wave loading of the structure. The blast wave, when impacting an object small compared to the shock wave surface, will seek the route of least energy or least resistance to propagate through. This can lead to a reduced loading experienced by the structure (or reduced duration and therefore impulse), due to this phenomena, also known as blast wave clearing. The second effect to be aware of from this blast wave clearing is that the distribution of the reflected pressure (force applied to the structure) varies across the structure from the centre to the boundary. The intensity of the blast wave will deteriorate towards the boundaries, where the wave is in close proximity to open-air. Conversely the boundaries closer to the ground can be expected to experience a greater initial loading (depending on the stand-off distance), due to shock wave reflections. To simplify the computational expense the effects of uneven loading, however, have been omitted from this study. The influence of the support (boundary) conditions on the target response is seen to be the most significant factor influencing the panel response and, so, formed the focus of the model.

For the experiments conducted on the CFRP, GFRP and mild steel test samples the supporting structure was also included in the model. Ideally, the composite plates would have rigid supports from the fixture. However, as this is not achievable in reality as observed experimentally. There is always a finite stiffness applied by the support. The method chosen was based on the same design as the steel test cubicle outlined in reference [14]. The test

fixture was modelled using an equivalent thickness of continuum shell elements. This was estimated considering the stiffness of the structural support elements (steel universal column and angle sections). The steel front was bolted onto concrete cast collets. The concrete did not move during testing and was therefore fixed in the model as a built-in boundary. The composite panels were then fixed to this plate.

The load was applied as a uniformly distributed pressure load based on the experimental measurements. During these experiments, overpressure was measured, therefore a conversion equation (taken from Chapter 3 of reference [17]) was used to convert the static pressure into the reflected pressure. The quality of this relationship was verified for peak measurements from previous experiments in which both static pressure and reflected pressure were recorded.

The skin configuration was changed by editing the section assignments of the sandwich panel from a GFRP to CFRP panel. The skins were changed to have the material properties as shown previously in Table 5.1. In addition to the GFRP and the CFRP targets, the steel sheet was also computed for completeness. The simulations were run to validate the model against the experimental data. These models were also intended to clarify that the savings made by using certain skin materials, with regard to blast resistance, is due to their performance and not a statistical anomaly. The number of experimental data points recorded for each test scenario is at most two. This is insufficient to conduct a classic statistical analysis on the experimental results. Therefore these models serve a purpose of verifying that the experimental results are statistically sound, if they form an agreement.

3.2. RESULTS

The results confirm the superior performance observed for the CFRP-skinned sandwich panels to the GFRP-skinned sandwich panels against air-blast loading. Figure 14 shows a comparison of the DIC analysis (experimental) of the blast on G25b and C25b with the FE data (numerical) overlaid for the central out-of-plane displacement. G25b and C25b are seen to deflect to a $U_{z,\max}$ of 150 mm and 110 mm respectively. This compares to the experimental results of 140 mm and 107 mm for G25b and C25b. The nature of the curves deviates after the initial impact to 1st maximum. This is due to a combination of target failures and boundary deformation, to be discussed further in the Section 3.3.

The contour plots from the numerical solution of the out-of-plane displacement are shown in Figure 15 with the predicted face deformation compared to DIC experimental date. This implies that a suitable model of this concrete/steel support structure is established such that the predictions of the simulation fall in line with the experimental. The samples were tested experimentally and numerically side-by-side and the displacement contours are displayed in Figure 15 side-by-side to emphasise the difference in performance of the two skin configurations (G25b and C25b). A further simulation was run of the steel sheet, S3a. The results of S3a will be introduced in Section 3.3.

3.3. ANALYSIS

From the comparison of experimental and modelling results shown above, a key parameter missing from the FEA implementation is a damage mechanism which can model accurately the core and skin damage observed. The increased damping would have slowed or inhibited the rebound stroke of the panel, eliminating the double peaks seen for C25b in Figure 14. In C25b the spread of core cracking was significantly higher than G25b, therefore this can account for why the impact on the numerical result of C25b was more apparent (for the lack

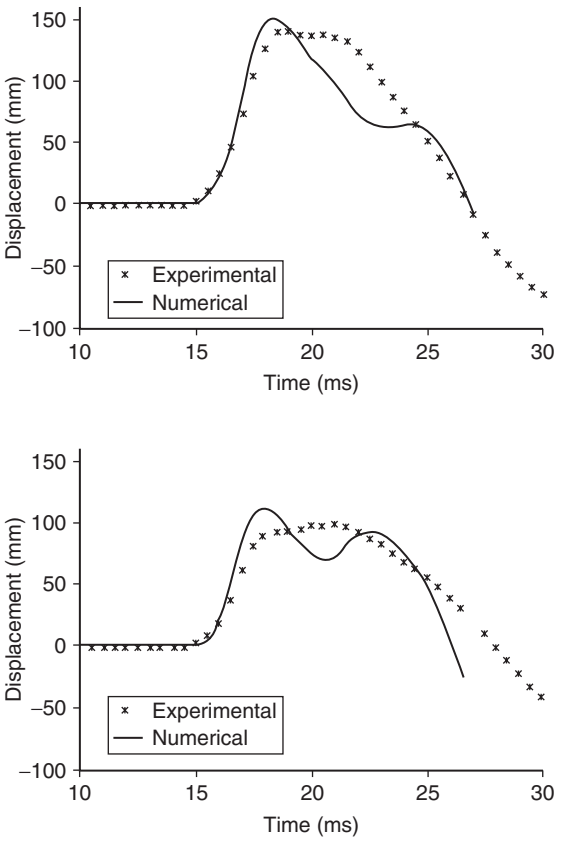

Figure 14 Two plots showing displacement-time history for both the experimental and numerical studies on the effect of skin configuration on sandwich panel response: *Top* is glass-fibre skinned sandwich panel - G25b and *Bottom* is carbon-fibre skinned sandwich panel - C25b. The blast parameters were 100 kg TNT equivalent at 14 m stand-off distance.

of a detailed core cracking model) than in G25b.

An indication of the impact such changes to this model could make is given in Figure 16. The graph shows the experimental results compared to the numerical results for S3a. When the elastic material model is used the model predicts a much stiffer target. Therefore an elastic perfectly-plastic material model was applied, taking the yield stress to be 331 MPa and the onset of plastic strain to be 1% as generic values for mild steel. This produces the third curve in Figure 16. The elastic perfectly-plastic model is a conservative model for the stiffening that occurs during dynamic events but was chosen for simplicity as an example. It is clear that the model is now more representative. Deviation occurs at 20 ms due to the energy released in bolt shear, which was not incorporated in the model.

A damage model is less important for understanding the response of the composite panels, as can be seen by comparing Figure 14 and Figure 16. This highlights the importance of considering the general characteristics of the materials modelled when deciding which factors will need to be included. The failure of the steel could be defined as global, as it

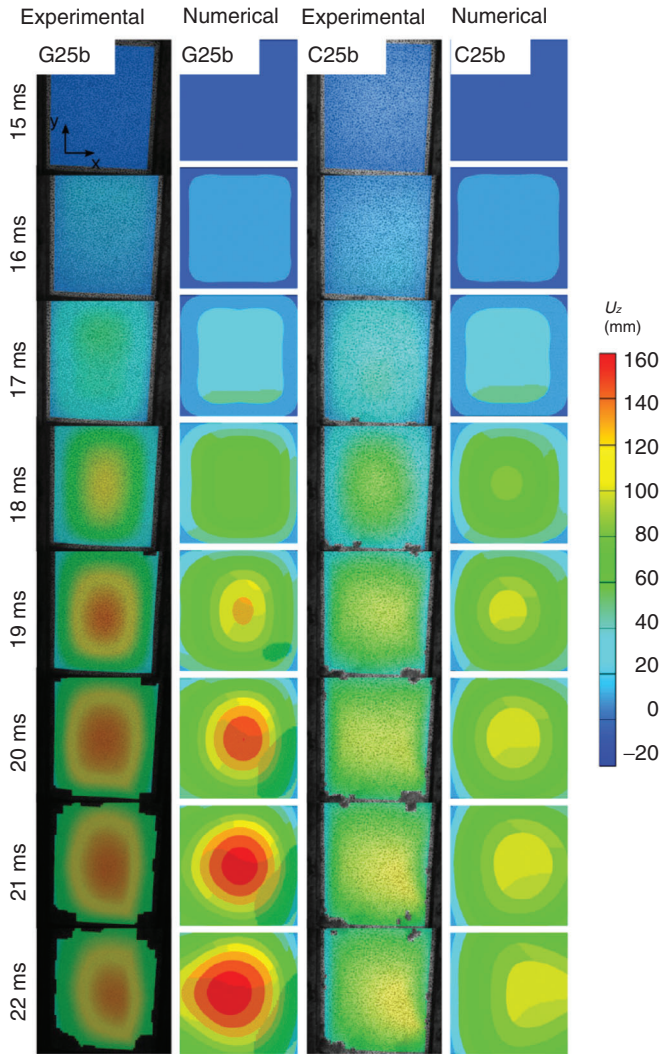

Figure 15 Blast summary for 100 kg TNT equivalent at 14 m stand-off for both G25b and C25b (1.3 m × 1.6 m exposed target area), displaying contour plots of the out-of-plane displacement from both experimental and finite element (Numerical) analyses.

affected the whole panel. Therefore, the numerical results without a damage model deviate very early on from the experimental results, particularly because the onset of plasticity occurs early in S3a too, and are unreliable to estimate the deformation behaviour. However the GFRP and CFRP panels' failures are more localised and occurred around $U_{z,\max}$. Therefore the model predicted the first deflection peaks, even though subsequent behaviour deviated from the recorded DIC results. The importance of assessing the appropriate level of accuracy in the material model is heightened especially when only a limited number of complications, in terms of support conditions, loading and material models, can practically be included.

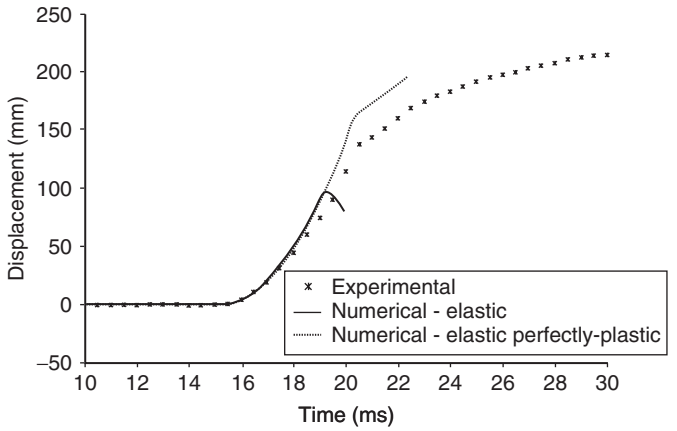

Figure 16 A plot showing the displacement-time history from both the experimental and numerical studies of the steel panel, S3a, response. An example of a simple damage material model is included for comparison to the purely elastic material model.

4. CONCLUSION

This paper has shown that increasing the stiffness of the panel for the same mass per unit area of the panel material is an important parameter in reducing damage generated. Both the experimental and modelling results have shown that the CFRP-skinned sandwich material perform best, in terms of exhibiting the lowest peak deflection and surface strains, in response to the same blast conditions. The CFRP skins showed little damage compared to the GFRP equivalent skins when panels were constructed of the same mass per unit area and thickness dimension. Core damage was comparable and further investigation is scheduled to section the samples to quantify the extent of damage and the levels of core damage between each sample. Failure in these composite sandwich panels tends to initiate in the transition region between the built-in corner and the central region of the panel which is flexing. In this transition region, shear strains develop between the front skin and the core, leading to a delamination which then propagated as a 45 degree shear crack through the core. The experimental trends for out of plane displacement were reproduced in the FE analysis. However, whilst the maximum values were comparable, the behaviour after the onset of expected/observed damage deviated. Damage mechanisms were not included for localised skin failures in the FRPCs but global failures were incorporated into the steel plate analysis, where they were seen more significant for representative analyses. This highlights the importance of using appropriate damage models in the simulations.

ACKNOWLEDGMENTS

Much appreciated is the support received from Dr Yapa Rajapakse of the Office of Naval Research (ONR N00014-08-1-1151) for Dr Hari Arora's PhD studies and S.P. GURIT & P.E. Composites for providing the composite panels.

REFERENCES

[1] Peles, S., Neuberger, A., and Rittel, D., Scaling the response of circular plates subjected to large and close-range spherical explosions. part i: Air-blast loading, *International Journal of Impact Engineering*, 2007, 34(5), 859–873.

[2] Peles, S., Neuberger, A., and Rittel, D., Scaling the response of circular plates subjected to large and close-range spherical explosions. part ii: buried charges, *International Journal of Impact Engineering*, 2007, 34(5), 874–882.

[3] Menkes, S.B. and Opat, H.J., Tearing and shear failure in explosively loaded clamped beams, *Experimental Mechanics*, 1973, 13(11), 480–486.

[4] Nurick, G.N. and Martin, J.B., Deformation of thin plates subject to impulsive loading - a review, part ii: Experimental studies, *International Journal of Impact Engineering*, 1989, 8(2), 171–186.

[5] Nurick, G.N., Olsson, M.D., and Fagnan, J.R., Deformation and rupture of blast loaded square plates - predictions and experiments, *International Journal of Impact Engineering*, 1993, 13(2), 279–291.

[6] Gelman, M.E., Nurick, G.N., and Marshall, N.S., Tearing of blast loaded plates with clamped boundary conditions, *International Journal of Impact Engineering*, 1996, 18(7–8), 803–827.

[7] Cantwell, W.J., Langdon, G.S., and Nurick, G.N., The blast response of novel thermoplastic-based fibre-metal laminates some preliminary results and observations, *Composites Science and Technology*, 2005, 65, 861–872.

[8] Nurick, G.N., et al., Behaviour of fibremetal laminates subjected to localised blast loading: Part i: experimental observations, *International Journal of Impact Engineering*, 2007, 34, 1202–1222.

[9] Nurick, G.N., et al., Behaviour of fibremetal laminates subjected to localised blast loading: Part ii: experimental observations, *International Journal of Impact Engineering*, 2007, 34, 1223–1245.

[10] Tekalur, S.A., Shukla, A., and Shivakumar, K., Blast resistance of polyurea based layered composite materials, *Composite Structures*, 2008, 84(3), 271–281.

[11] Tekalur, S.A., Shivakumar, K., and Shukla, A., Mechanical behavior and damage evolution in E-glass vinyl ester and carbon composites subjected to static and blast loads, *Composites Part B*, 2008, 39(1), 57–65.

[12] Tekalur, S.A., Bogdanovich, A.E., and Shukla, A., Shock loading response of sandwich panels with 3-D woven E-glass composite skins and stitched foam core, *Composites Science and Technology*, 2009, 69(6), 736–753.

[13] Arora, H., Hooper, P., and Dear, J., The Effects of Air and Underwater Blast on Composite Sandwich Panels and Tubular Laminate Structures, *Experimental Mechanics*, 2012, 52(1), 59–81.

[14] Arora, H., Hooper, P.A., and Dear, J.P., Dynamic response of full-scale sandwich composite structures subject to air-blast loading, *Composites Part A: Applied Science and Manufacturing*, 2011, 42(11), 1651–1662.

[15] Hooper, P.A., Sukhram, R.A.M, Blackman, B.R.K. and Dear, J.P., On the blast resistance of laminated glass, *International Journal of Solids and Structures*, 2012, 49(6), 899-918.

[16] Biggs, J.M., *Introduction to Structural Dynamics*, McGraw-hill Publishing Company, USA, 1964.

[17] Smith, P.D. and Hetherington, J.G., *Blast and ballistic loading of structures*, Butterworth Heinmann, 1994.